

mK-STM Studies of the Temperature- and Field-dependence of the Quasiparticle Spectrum of Sr₂RuO₄

C. Lupien,^{1,*} S. K. Dutta,² B. I. Barker,³ Y. Maeno,⁴ and J. C. Davis^{1,†}

¹*Department of Physics, LASSP, Cornell University, Ithaca NY 14853, USA.*

²*Department of Physics, University of Maryland, College Park, MA 20742, USA.*

³*Laboratory for Physical Sciences, University of Maryland, College Park, MA 20740, USA.*

⁴*Department of Physics, Kyoto University, Kyoto 606-8502, JAPAN.*

(Dated: November 13, 2018)

Atomic-resolution scanning tunneling spectroscopy is used to study the spectrum of quasiparticle states in superconducting Sr₂RuO₄. The measured temperature dependence of the quasiparticle spectrum is consistent with a multi-band superconducting order parameter with one band exhibiting a line of nodes, if a constant density of states offset can be ascribed to a surface effect. In magnetic fields $H < H_{c2}$, a vortex lattice, square and oriented parallel to the $\langle 110 \rangle$ direction of the RuO₂ lattice, is detected by spectroscopic imaging. Each vortex exhibits one flux quantum and a strong zero-bias conductance peak.

PACS numbers: 68.37.Ef, 74.20.Rp, 74.70.Pq

Sr₂RuO₄ displays an exotic form of superconductivity at temperatures below 1.45 K [1, 2]. Because of the independence of the spin susceptibility on temperature below T_c [3, 4, 5], the Cooper pairs are believed to be in a spin triplet ‘equal spin pairing’ (ESP) state. Muon spin rotation studies also show a time-reversal-symmetry breaking (spontaneous magnetization) signal which is also consistent with spin-triplet superconductivity [6].

Many discussions have proceeded in terms of a purely 2-dimensional version of the p -wave order parameter (OP) $\mathbf{d} = \Delta \hat{\mathbf{z}}(k_x \pm ik_y)$. But it now appears that the Sr₂RuO₄ OP is somewhat more complex than this. It has recently emerged that (i) the low temperature electronic heat capacity C_e [7], (ii) the nuclear spin relaxation time [8], (iii) the thermal conductivity [9], (iv) the London penetration depth [10] and (v) the ultrasound attenuation [11] have low temperature power laws which are consistent with the presence of line nodes (Fig. 1b).

A microscopic model consistent with these observations has also recently emerged. In Sr₂RuO₄, three electronic bands cross the Fermi level leading to three closed Fermi-sheets in momentum space: α (X centered hole-like), β and γ (Γ centered electron like) [12, 13]. It is proposed that on the γ sheet the superconductivity is dominant while the remaining two sheets have induced superconducting gaps [14, 15]. Although this model of Sr₂RuO₄ is elegant, plausible, and consistent with experiments, it is by no means certain [2].

Tunneling spectroscopy has historically played a key role in the study of superconductivity [16]. This is because the differential tunneling conductance $g = dI/dV$ at bias voltage V_b between a sample and metal tip is proportional to the sample local density of quasiparticle states (LDOS) at energy $E = eV_b$; $g(\mathbf{r}, V_b) \propto \text{LDOS}(\mathbf{r}, E = eV_b)$. Scanning tunneling spectroscopic imaging has further advanced the utility of this technique by allowing mapping throughout space of $g(\mathbf{r}, V_b)$. For

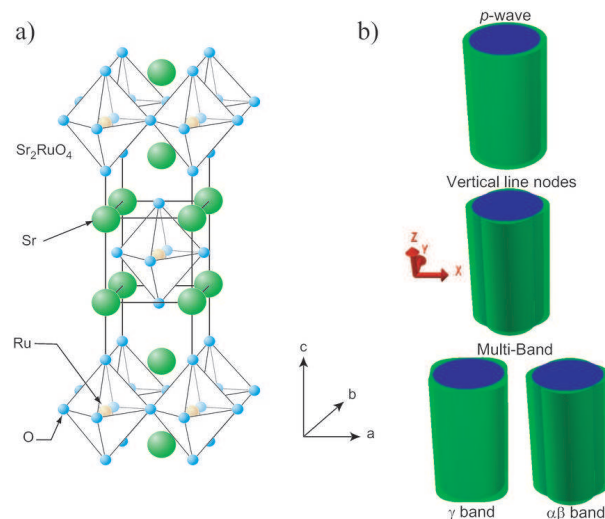


FIG. 1: a) Crystal structure of Sr₂RuO₄. b) Schematic of various gap order: top is a p -wave, middle is vertical line nodes and at the bottom is a multi-band model with both a modulated p -wave and vertical line nodes on different Fermi surfaces.

example, in s -wave NbSe₂, the vortex lattice and core structure have been determined with this technique [17], and in d -wave cuprate superconductors it has revealed the vortex structure [18], nanoscale electronic disorder [19], impurity atom effects [20], and quasiparticle quantum interference [21]. In this paper we apply these techniques to Sr₂RuO₄.

Several important STM studies of Sr₂RuO₄ have already been reported. At temperatures high compared to T_c , topographic imaging of surface structure reveals unexpected reconstructions of SrO surface [22]. Tunneling spectroscopy has been carried out below T_c but on an unidentified, and ramified, surface yielding the unexpected result that the LDOS at $E = 0$ was about 90%

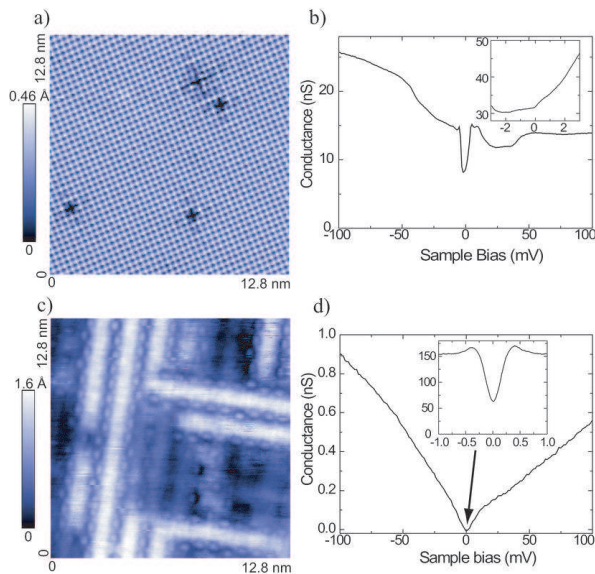


FIG. 2: a) Topographic image of a Ti doped sample showing the usual square and uniform lattice (and some Ti impurities). b) Spectra taken on the surface a) away from a Ti atom showing a 50 mV and a 10 mV gaps. The inset shows that there is no superconducting feature seen at low energy. c) Topographic image taken on the pure sample studied here showing a very different surface structure. d) spectra taken on the image of c) and showing a very different V-like spectra with weak features (small slope changes) at 50 and 10 mV and reaches a very small conductance around zero bias. The inset shows data taken at small bias voltage (± 1 mV) showing the superconducting gap. The topographs were taken with a setpoint of 100 mV and 0.05 nA.

of normal value even at low temperature [23]. A possible explanation was the level of disorder seen in the images. Nonetheless, this study was an important advance since it detected a partially gapped quasiparticle spectrum.

We use a dilution-refrigerator based STM which reaches 15 mK in fields up to 8.5 T with atomic-resolution scanning tunneling spectroscopy. This system also allows samples to be cleaved in cryogenic ultra high vacuum inside the vacuum space of the dilution refrigerator and then immediately inserted into the STM head mounted below the mixing chamber. We use floating-zone-fabricated Sr_2RuO_4 single crystals which have $T_c=1.45$ K.

In Sr_2RuO_4 , this cleavage technique can, in principle, result in two c -axis normal crystalline surface layers: the SrO layer and the RuO_2 layer (see crystal structure in Fig. 1a). Topographic images of two surface types we observe are shown in Fig. 2a and Fig. 2c. The first surface layer was identified as being SrO using Ti atom substitution experiments [24]. This surface never exhibits a superconducting quasiparticle spectrum but instead shows the spectrum in Fig. 2b.

A topographic image of a second type of cryo-cleave

surface (likely RuO_2) is shown in Fig. 2c. This image shows a quasi-one-dimensional structure on this surface. The width of the “bands” in the figure are $4a_0$ (where a_0 is the in-plane lattice constant, 0.386 nm) while the periodicity of the “beads” running the length of the “bands” is $2a_0$. Domains of both orientations of the quasi 1-d topographic structure are clearly seen everywhere on this surface. Surface reconstruction effects that are sensitive to the cleaving recipe have been seen in some measurements [22, 25, 26]. It is not clear how these high temperature cleaved reconstructions are related to the one reported here.

Independent of structural details of this RuO layer reconstruction, the surface shown in Fig. 2c displays a differential tunneling conductance spectrum as shown in Fig. 2d, and with high resolution in Fig. 3a). We have studied the spectrum over regions up to $1.1 \mu\text{m}^2$ and it is highly repeatable and reliable, having almost identical characteristics independent of exact atomic details of surface reconstruction.

We carried out the following tests to demonstrate that these spectra represent the superconducting quasiparticle spectrum of Sr_2RuO_4 . First, the temperature dependence studies show the observed gap disappears at T_c (see Fig. 3b) filling from 40% to 100% of normal LDOS($E=0$). Second, at millikelvin temperatures, this gapped spectrum has disappeared at a magnetic field of $\mu_0 H = 100$ mT, which is very close to the c -axis H_{c2} of the superconducting state. Third, in the presence of fields $H < H_{c2}$ this spectrum shows the characteristic spatial variations expected from the core of vortices exhibiting ϕ_0 of magnetic flux (see Fig. 4). We therefore conclude that we are dealing primarily with the quasiparticle spectrum of superconducting OP of Sr_2RuO_4 .

To analyze the shape of the spectra and their temperature dependence we consider three different models of OP; an isotropic p -wave gap

$$\Delta(\phi) = \Delta_0^p e^{\pm i\phi}, \quad (1a)$$

a gap with a vertical line of nodes

$$\Delta(\phi) = \Delta_0^{\text{line}} e^{\pm i\phi} \sin(2\phi), \quad (1b)$$

and a modulated p -wave gap (which is combined with vertical line nodes for the multi-band model):

$$\Delta(\phi) = \Delta_0^{\text{p-mod}} e^{\pm i\phi} \left[1 - \frac{\alpha}{2} - \frac{\alpha}{2} \cos(4\phi) \right]. \quad (1c)$$

In this latter case, the in-plane modulation of the gap along ϕ has peak-to-peak amplitude of α (i.e. a maximum of 1 and a minimum of $1 - \alpha$).

The local conductance $g(\mathbf{r}, V_b, T)$ is obtained from the local density of states of the various gap models (Eq. 1a-1c) by including thermal smearing T . Therefore predictions for the differential tunnel conductance of the gaps

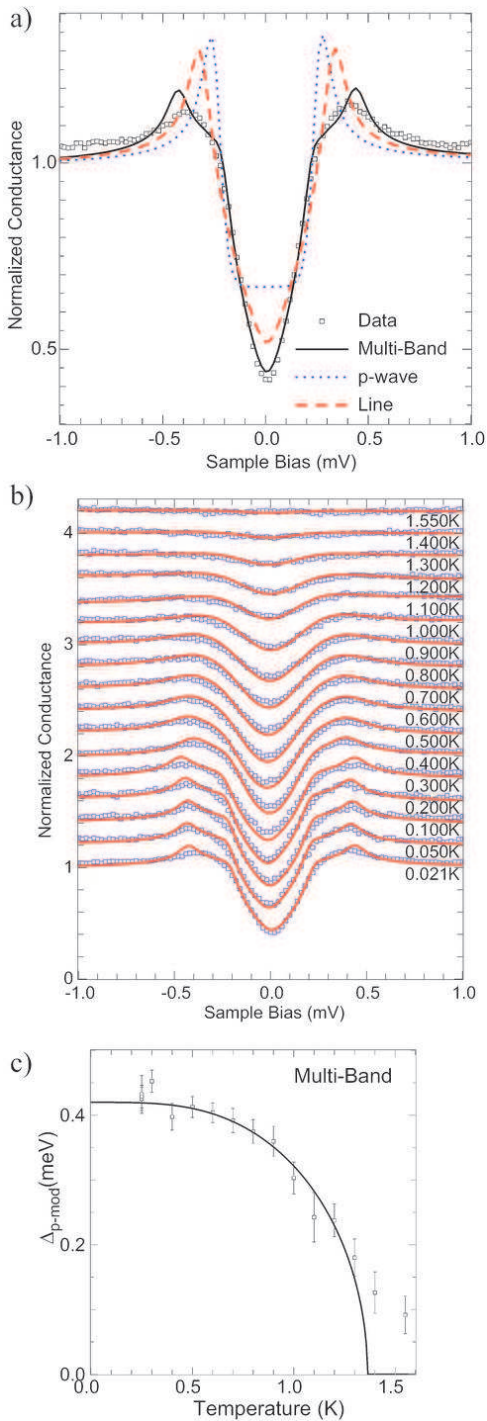


FIG. 3: a) Shows three different fits to the lowest temperature conductance data. The dotted (blue) line is for an isotropic p -wave gap. The dashed (red) line is for vertical line nodes and the solid (black) line is for the multi-band model discussed in the text. b) Temperature dependence of the data and the associated multi-band model fits. The different temperatures are shifted vertically for clarity. c) The $\Delta_{p\text{-mod}}$ gap parameter obtained from the fit in b) compared with a BCS like temperature dependence shown by the line (Δ_{line} is kept a constant fraction of $\Delta_{p\text{-mod}}$ hence has the same temperature dependence).

are obtained as $g_p(V)$ (which could as well represent an s -wave OP), $g_{\text{line}}(V)$ and $g_{p\text{-mod}}(V)$. Note that horizontal line nodes ($\Delta_0 \cos(k_z c)$) gives the same conductance as vertical line nodes, and that the orientation of the nodes as well as the $\exp(\pm i\phi)$ part of the gaps also does not modify the conductance.

To relate the three models to the measured conductance $g(\mathbf{r}, V_b)$ in the experiment (Fig. 3a), we fit the data to a general form which includes a background density of states which is added as a fraction f of the total conductance,

$$g(V) = A \left[(1 - f) G(V) + f \right] \quad (2)$$

and for the multi-band model

$$g(V) = A \left\{ (1 - f) [(1 - x) g_{\text{line}}(V) + x g_{p\text{-mod}}(V)] + f \right\} \quad (3)$$

where V is the bias voltage, A is the amplitude of the conductance and G is either g_{line} or g_p . We consider f , which is about 40%, to be a spurious effect. This is reasonable since heat capacity experiments show the number of thermally occupied states in bulk falling precipitously at these low temperatures. In case of the multi-band model, x is the fraction of the non-background LDOS due to the modulated p -wave gap (the γ band). Therefore we have 2 or 3 adjustable parameters (A , f and x) in addition to the predicted $g(V)$ of the gap function of interest. The temperature is fixed to the measured sample temperature, except at very low temperatures below 250 mK where we fix the temperature to 250 mK because (1) we believe from independent studies that this tip did not cool below that temperature and (2) this is the sample temperature at which the measured spectra start changing.

As can be seen in Fig. 3a, the simplest p -wave fit $G = g_p$ is quite poor compared to the line nodes. The multi-band model is better than a pure line nodes model (possibly because of the larger number of parameters). Other gap-models with extra parameters over a simple line node also fit as well, such as a modulated horizontal line of nodes: $\Delta_0 \cos(k_z c) [1 - \beta \cos(4\phi)]$ (but this would fail to reproduce the heat capacity jump at T_c). The particular multi-band model was selected because it is consistent with a recent study of the dependence of the heat capacity on the angle of the magnetic field [27]. We caution that the value of x is controlled not only by the density of states of the different bands but also by the tunneling matrix element.

We next study the temperature dependence of these tunneling spectra. In Fig. 3b, we show averaged spectra taken at the 17 temperatures between 20 mK and 1.6 K. They were obtained after averaging about 100 individual spectra (25 s each) with a bias modulation of $20 \mu\text{V}_{\text{RMS}}$ and setpoints of 10 mV / 0.25 nA or 5 mV / 0.15 nA. Different locations were used for data acquisition at each

temperature. The solid lines in Fig. 3b are the result of fits to the multi-band model. The lowest temperature is fitted the same way as in Fig. 3a above. For all other temperatures f , x and α are kept constant at their low temperature value (0.38, 0.30 and 0.37 respectively), T is set to the measurement temperature but $\Delta_0^{\text{p-mod}}$ is left to evolve while keeping the ratio $\Delta_0^{\text{p-mod}}/\Delta_0^{\text{line}}$ fixed to the low temperature value of 1.9.

From all these fits, a temperature dependence of the gap $\Delta_0^{\text{p-mod}}$ can be extracted and the result is shown in Fig. 3c where the solid curve is a fit to a BCS temperature dependence of the gap. A very similar graph is obtained if a vertical line nodes model is used.

A second important use of spectroscopic mapping is in the determination of effects of magnetic field on the superconducting OP. This can be very revealing since the structure of the vortex lattice and the electronic structure of the core are closely related to the symmetry of the OP. For the case of a p -wave OP, a number of theoretical studies [28, 29, 30, 31] have explored the predicted structure of the vortex core in 2-d OP $\mathbf{d} = \Delta\hat{\mathbf{z}}(k_x \pm ik_y)$.

Experimentally, the flux lattice has been measured by small angle neutron scattering [32]. However, until the present work, nothing is known about the local electronic structure of Sr_2RuO_4 vortex cores. To explore these issues we mapped point spectra at >140 individual locations in $B < \mu_0 H_{c2}$. We detected 5 vortices with mean separation between cores of 180 ± 30 nm. Within our statistical uncertainty, the lattice is square and oriented parallel to the $\langle 110 \rangle$ axes of the crystal lattice which is quite consistent with previous neutron studies. We detect the vortices from the changes in $g(\mathbf{r}, 0)$ at the vortex center, forming a pattern consistent with a square lattice and the separation of the core locations at $B = 50$ mT yields a flux $\Phi = 1 \pm 0.15\Phi_0$ threading each core.

To study the Sr_2RuO_4 vortex core itself, we measure $g(\mathbf{r}, V)$ at regions nearby the core (Fig. 4a) and along lines connecting two cores (crystallographic $\langle 110 \rangle$ direction) as shown in Fig. 4b. The most striking feature is the very strong zero bias conductance peak (ZBCP) of FWHM $250 \mu\text{eV}$ and maximum intensity 115% of the normal density of states. The coherence length can also be estimated from decay length of the gap suppression away from the core to be 50 nm in reasonable agreement with the estimate of 65 nm from penetration depth studies.

A number of important conclusions can be drawn. First, the RuO surface of Sr_2RuO_4 exhibits a gapped, particle-hole symmetric, density of states spectrum consistent with a superconductor. Second, the temperature dependence of the observed $g(\mathbf{r}, E)$ is best fit by a superconducting multi-band gap with at least one band supporting a line of nodes [33]. This provides further corroboration for this picture of the gap structure in Sr_2RuO_4 . Third, direct imaging of the vortex lattice by spectro-

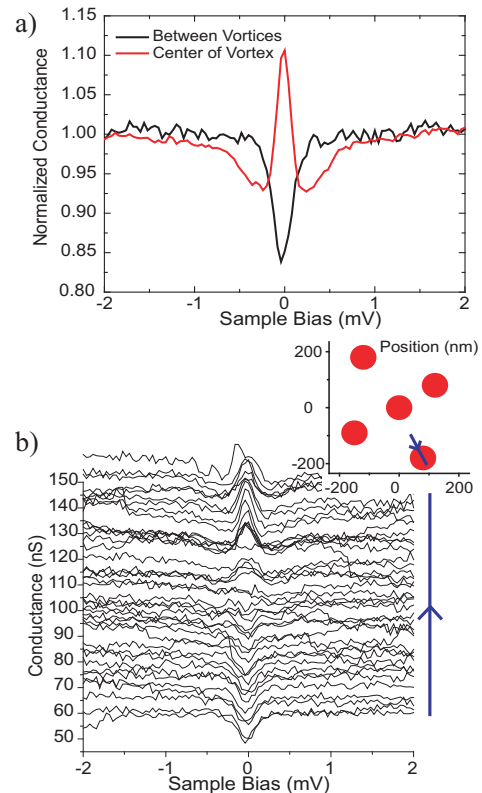


FIG. 4: a) Averaged point spectra at the center (red) and in between (black) vortex showing the ZBCP at the center. b) Line cut through a vortex (as shown in the inset). The inset also shows the location of the 5 places where we identified a vortex core. The data was taken with a setpoint of 2 mV and 0.15 nA.

scopic mapping is now possible. Because of this, the long mooted experiment to search for chiral domains that can exist in a $k_x \pm ik_y$ OP [34], becomes technically feasible. Finally, the large ZBCP discovered in Sr_2RuO_4 is consistent with p -wave models that did not consider line nodes. It will require new theoretical models to understand the ZBCP in a multi band model.

This work was supported by the ONR grant N00014-03-1-0674, NSF grant NSF-ITR FDP-0205641, ARO grant DAAD19-02-1-0043 and MEXT of Japan. C.L. acknowledges support from NSERC.

* Department of Physics, Université de Sherbrooke, Sherbrooke, Qc J1K 2R1, Canada.

† Electronic address: jcdavis@ccmr.cornell.edu

- [1] Y. Maeno *et al.*, Nature (London) **372**, 532 (1994).
- [2] A. P. Mackenzie and Y. Maeno, Review of Modern Physics **75**, 657-712 (2003).
- [3] K. Ishida *et al.*, Nature (London) **396**, 658 (1998).
- [4] K. Ishida *et al.*, Phys. Rev. B **63**, 060507(R) (2001).
- [5] J. A. Duffy *et al.*, Phys. Rev. Lett. **85**, 5412 (2000).

- [6] G. M. Luke *et al.*, Nature (London) **394**, 558 (1998).
- [7] S. Nishizaki, Y. Maeno, and Z. Q. Mao, J. Phys. Soc. Jpn. **69**, 572 (2000).
- [8] K. Ishida *et al.*, Phys. Rev. Lett. **84**, 5387 (2000).
- [9] M. A. Tanatar *et al.*, Phys. Rev. B **63**, 064505 (2001); M. A. Tanatar *et al.*, Phys. Rev. Lett. **86**, 2649 (2001); K. Izawa *et al.*, Phys. Rev. Lett. **86**, 2653 (2001).
- [10] I. Bonalde *et al.*, Phys. Rev. Lett. **85**, 4775 (2000).
- [11] C. Lupien *et al.*, Phys. Rev. Lett. **86**, 5986 (2001).
- [12] C. Bergemann *et al.*, Phys. Rev. Lett. **84**, 2662 (2000); C. Bergemann *et al.*, Physica B **294**, 371 (2001).
- [13] A. Damascelli *et al.*, Phys. Rev. Lett. **85**, 5194 (2000); Comment Reply: Phys. Rev. Lett. **87**, 239702 (2001).
- [14] D. F. Agterberg, T. M. Rice, and M. Sgrist, Phys. Rev. Lett. **78**, 3374 (1997).
- [15] M. E. Zhitomirsky, and T. M. Rice, Phys. Rev. Lett. **87**, 057001 (2001).
- [16] W. L. McMillan and J. M. Rowell, Superconductivity, edited by R. D. Parks Volume 1 chapter 11 pages 561-614 (1969).
- [17] H. F. Hess *et al.*, Phys. Rev. Lett. **62**, 214 (1989).
- [18] J. E. Hoffman *et al.*, Science **295**, 466 (2002).
- [19] V. Madhavan *et al.*, Bull. Amer. Phys. Soc. **45**, 416 (2000).; S. H. Pan, *et al.*, Nature **413**, 282 (2001); K. M. Lang *et al.*, Nature **415**, 412 (2002).
- [20] E. W. Hudson *et al.*, Science **285**, 88 (1999) ; S. H. Pan *et al.*, Nature **403**, 746 (2000) ; E. W. Hudson *et al.*, Nature **411**, 920 (2001).
- [21] K. McElroy *et al.*, Nature (London) **422**, 592 (2003).
- [22] R. Matzdorf *et al.*, Science **289**, 746 (2000).
- [23] M. D. Upward *et al.*, Phys. Rev B **65**, 220512(R) (2002); H. Kambara *et al.*, Physica C **388-389**, 503 (2003).
- [24] B. I. Barker *et al.*, Physica B **329-333**, 1334 (2003)
- [25] R. Matzdorf *et al.*, Phys. Rev. B **65**, 085404 (2002).
- [26] K. M. Shen *et al.*, Phys. Rev. B **64**, 180502(R) (2001).
- [27] K. Deguchi, Z. Q. Mao, H. Yaguchi, and Y. Maeno, Phys. Rev. Lett. **92**, 047002 (2004); K. Deguchi, Z. Q. Mao, Y. Maeno, J. Phys. Soc. Jpn **73**, 1313 (2004).
- [28] L. Tewordt and T. Dahm, Phys. Rev. B **63**, 092505 (2001).
- [29] M. Takigawa *et al.*, Phys Rev B. **65**, 014508 (2001).
- [30] K. Maki *et al.*, Physica C **317-318**, 353 (1999).
- [31] M. Ichioka and K. Machida, Phys. Rev. B **65**, 224517 (2002).
- [32] T. M. Riseman *et al.*, Nature **396**, 242 (1998); correction in **404**, 629 (2000).
- [33] T. Nomura and K. Yamada, J. Phys. Soc. Jpn **71**, 404 (2002); Y. Yanase *et al.*, Phys. Rep. **387**, 1 (2003).
- [34] E. Dumont and A. C. Mota, Phys. Rev. B **65**, 144519 (2002).